

Giant Correlated Gap and Possible Room-Temperature Correlated States in Twisted Bilayer MoS₂

Fanfan Wu,^{1,2} Qiaoling Xu,^{3,4} Qingqin Wang[ⓧ],^{1,2} Yanbang Chu,^{1,2} Lu Li,^{1,2} Jian Tang,^{1,2} Jieying Liu,^{1,2} Jinpeng Tian[ⓧ],^{1,2} Yiru Ji,^{1,2} Le Liu,^{1,2} Yalong Yuan,^{1,2} Zhiheng Huang,^{1,2} Jiaojiao Zhao,^{1,2} Xiaozhou Zan,^{1,2} Kenji Watanabe[ⓧ],⁵ Takashi Taniguchi,⁶ Dongxia Shi,^{1,2,3} Gangxu Gu,^{1,2} Yang Xu[ⓧ],^{1,2} Ledex Xian,^{3,*} Wei Yang,^{1,2,3,†} Luojun Du[ⓧ],^{1,2,‡} and Guangyu Zhang^{1,2,3,§}

¹Beijing National Laboratory for Condensed Matter Physics, Institute of Physics, Chinese Academy of Sciences, Beijing 100190, China


²School of Physical Sciences, University of Chinese Academy of Sciences, Beijing 100049, China

³Songshan Lake Materials Laboratory, Dongguan, Guangdong 523808, China

⁴College of Physics and Electronic Engineering, Center for Computational Sciences, Sichuan Normal University, Chengdu 610068, China

⁵Research Center for Functional Materials, National Institute for Materials Science, 1-1 Namiki, Tsukuba 305-0044, Japan

⁶International Center for Materials Nanoarchitectonics, National Institute for Materials Science, 1-1 Namiki, Tsukuba 305-0044, Japan

 (Received 30 January 2023; revised 21 August 2023; accepted 21 November 2023; published 18 December 2023)

Moiré superlattices have emerged as an exciting condensed-matter quantum simulator for exploring the exotic physics of strong electronic correlations. Notable progress has been witnessed, but such correlated states are achievable usually at low temperatures. Here, we report evidence of possible room-temperature correlated electronic states and layer-hybridized SU(4) model simulator in AB-stacked MoS₂ homobilayer moiré superlattices. Correlated insulating states at moiré band filling factors $\nu = 1, 2, 3$ are unambiguously established in twisted bilayer MoS₂. Remarkably, the correlated electronic state at $\nu = 1$ shows a giant correlated gap of ~ 126 meV and may persist up to a record-high critical temperature over 285 K. The realization of a possible room-temperature correlated state with a large correlated gap in twisted bilayer MoS₂ can be understood as the cooperation effects of the stacking-specific atomic reconstruction and the resonantly enhanced interlayer hybridization, which largely amplify the moiré superlattice effects on electronic correlations. Furthermore, extreme large nonlinear Hall responses up to room temperature are uncovered near correlated electronic states, demonstrating the quantum geometry of moiré flat conduction band.

DOI: [10.1103/PhysRevLett.131.256201](https://doi.org/10.1103/PhysRevLett.131.256201)

Moiré superlattices formed by vertically stacking atomic layers with a twist and/or a lattice mismatch, introduce a new length and energy scale to engineer the electronic structure and represent a highly controllable quantum platform for a wide variety of emerging correlated physics [1–5]. One well-known manifestation is magic-angle twisted bilayer graphene, where the formation of moiré flat bands strongly enhances the ratio U/W by significantly suppressing W (U and W are electron-electron interaction and electronic bandwidth, respectively) and hence results in a rich phase diagram of correlated electronic states, such as Chern insulator states [6–9], orbital ferromagnetism [10,11], and unconventional superconductivity [10,12,13]. However, because U is considerably small (~ 10 meV) [5], these correlated states in the twisted graphene system can survive only at temperatures of a few K, limiting their tunability in experiments and hindering their applications in quantum technologies. Therefore, it is particularly important to explore additional

moiré superlattices with large U , which may enable the possibilities of correlated electronic states at high temperatures.

Given that U is inversely proportional to the dielectric constant, transition metal dichalcogenide (TMD) moiré superlattices with relatively small dielectric constants represent a potential platform to realize high-temperature correlated physics [2,14]. Indeed, a host of correlated electronic states, such as generalized Wigner crystal states, excitonic insulator, quantum criticality, and quantum anomalous Hall effect have been uncovered in TMD homo- and heterostructure superlattices at much higher critical temperatures than in graphene moiré superlattices [15–23]. Notably, correlated phases up to about 150 K have been realized at half filling of the first moiré miniband in angle-aligned WSe₂/WS₂ and MoSe₂/WS₂ moiré superlattices [24,25]. The critical temperatures of correlated electronic states in these TMD heterostructure superlattices, although significantly increased compared to that

in graphene moiré superlattices, are still well below room temperature.

In this work, we fabricate high-quality, encapsulated, dual-gated MoS₂ homobilayer moiré superlattice devices and report the transport evidences of possible room-temperature correlated electronic states in AB stacked samples with a twist angle of $\sim 57.5^\circ$. Insulating states at doping density of one, two, and three electrons per moiré superlattice site are uncovered unambiguously. Together with first-principle calculations, we uncover that these insulating states correspond to correlated electronic phases at moiré band filling factors $\nu = 1, 2, 3$, evidencing a layer-hybridized SU(4) correlated model simulator. This is in sharp contrast to previous TMD moiré superlattice results of single-band SU(2) Hubbard model that correlation-induced insulating phases can appear only at half-filling of moiré band. Notably, $\nu = 1$ correlated state hosts a record-large correlated gap of ~ 126 meV and may persist up to a record-high temperature over 285 K, demonstrating ultra-strong electron correlations in MoS₂ homobilayer moiré superlattice. Furthermore, large nonlinear Hall responses up to room temperature are uncovered near the correlated electronic states, demonstrating the quantum geometrical properties of electron wavefunctions.

Correlated electronic states in twisted bilayer MoS₂.—It is well known that the direct electrical-transport detection of the correlated states is challenging in TMD semiconductor moiré superlattices [16,26]. To construct high-quality moiré superlattices for transport measurements, we adopt monolayer MoS₂ single crystals grown by the van der Waals epitaxial technique, which show better electronic qualities than the exfoliated ones (Supplemental Material Fig. 1 [27]) [28,29]. Then hexagonal boron nitride (*h*-BN) encapsulated, dual-gated MoS₂ homobilayer moiré superlattice devices with multiple electrodes are fabricated utilizing the “cut and stack” technique [37,38]. Figure 1(a) shows the schematic diagram of the twisted bilayer MoS₂ dual-gate device. The twist angles are controlled to be at $\sim 57.5^\circ$ (i.e., AB stacking) or $\sim 2.5^\circ$ (i.e., AA stacking), producing a moiré superlattice with a periodicity close to 7–8 nm [Fig. 1(b)]. The long periodic moiré potential would fold the band into the mini-Brillouin zone [Fig. 1(c)]. Few-layer graphene less than 1 nm is used as the contact to MoS₂, which can endow good Ohmic contact and facilitate the cryogenic transport [39]. Moreover, the dual-gate configuration enables us to independently tune the carrier density n and out-of-plane displacement field \mathbf{D} . Here $n = (C_b V_b + C_t V_t)/e$ and $\mathbf{D} = (C_b V_b - C_t V_t)/2\epsilon_0$, where e (ϵ_0) is the elementary charge (vacuum permittivity), C_b (V_b) and C_t (V_t) are the geometrical capacitances per area (applied voltages) for the bottom and top gates, respectively.

Figure 1(e) shows the color plot of four-terminal longitudinal resistance as a function of n at various temperatures for 57.15° twisted bilayer MoS₂ (device No. 1). The

corresponding optical image can be found in Fig. 1(d) and Supplemental Material Fig. 4 [27]. It is noteworthy that although one of the MoS₂ layers is closely aligned to the top *h*-BN layer in device No. 1 (Supplemental Material Fig. 4 [27]), the aligned effect on band structures and electronic correlations can be ignored because of large lattice mismatch ($\sim 25\%$). Unless otherwise specified, all results in the main text are taken from device No. 1. Remarkably, apart from the diverging resistance peaks at $n = 0$ that mark the intrinsic band edge of MoS₂, four strong resistance peaks at $n = n_0, 2n_0, 3n_0, 4n_0$ are clearly observed. $n_0 = 2.85 \times 10^{12}$ cm⁻² is equal to $1/A$ and thus corresponds to moiré density that one electron per superlattice site, where $A = (\sqrt{3}/8)(a^2/\{\sin[(60 - \theta)/2]\}^2)$ denotes the moiré unit cell area with $a = 0.315$ nm (θ) the MoS₂ lattice constant (twist angle). In other words, the four strong resistance peaks at $n = n_0, 2n_0, 3n_0, 4n_0$ coincide with one, two, three, four electrons per moiré superlattice site—that is, moiré band filling factors $\nu = 1, 2, 3, 4$. Figure 1(f) shows a plot of the resistance versus n for five different twisted bilayer MoS₂ devices. All the five devices exhibit apparent resistance peaks at moiré band filling factors $\nu = 1, 2, 3$. The weak insulating state at $\nu = 4$ is because the measuring temperature is above 20 K.

To gain more insight of these insulating states, we perform density functional theory (DFT) calculations on commensurate 56.85° twisted bilayer MoS₂. Additional DFT calculations on other twist angles can be found in the Supplemental Material Fig. 11 [27]. The calculated band structure with considering layer hybridization is shown in Fig. 1(g) (see details in the Supplemental Material [27]). Clearly, ultraflat moiré minibands emerge at the conduction band bottom with a bandwidth less than 10 meV (Fig. 8 in [27]). The flat moiré minibands are contributed from the original $\pm K$ valley states of the two constituent MoS₂ layers, as confirmed by their charge density distribution (Fig. 10 in [27]). Because of negligible spin-orbit coupling (only ~ 3 meV) [40], four spin-degenerate states from the $\pm K$ valleys of the two constituent layers are folded to moiré mini-Brillouin zone [Fig. 1(c)]. With atomic reconstruction in moiré scale, eightfold degenerate flat minibands are formed (including two spin, two valley, and two layer) when the layer hybridization is artificially turned off [Fig. 1(h)]. Owing to the perfect band alignment, interlayer hybridization is resonantly enhanced in twisted bilayer MoS₂. After turning on the layer hybridization, the eightfold degenerate flat minibands split into two sets of fourfold degenerate flat minibands as layer bonding and antibonding orbitals [Fig. 1(g) and Supplemental Material Fig. 9 [27]]. Consequently, the resistance peak at $\nu = 4$ can be well understood as the full filling of first flat moiré miniband with a reduction in the density of states. By contrast, the insulating states at $\nu = 1, 2, 3$ correspond to the partial fillings of the first moiré flat miniband and defy the description by single-particle band structure paradigm.

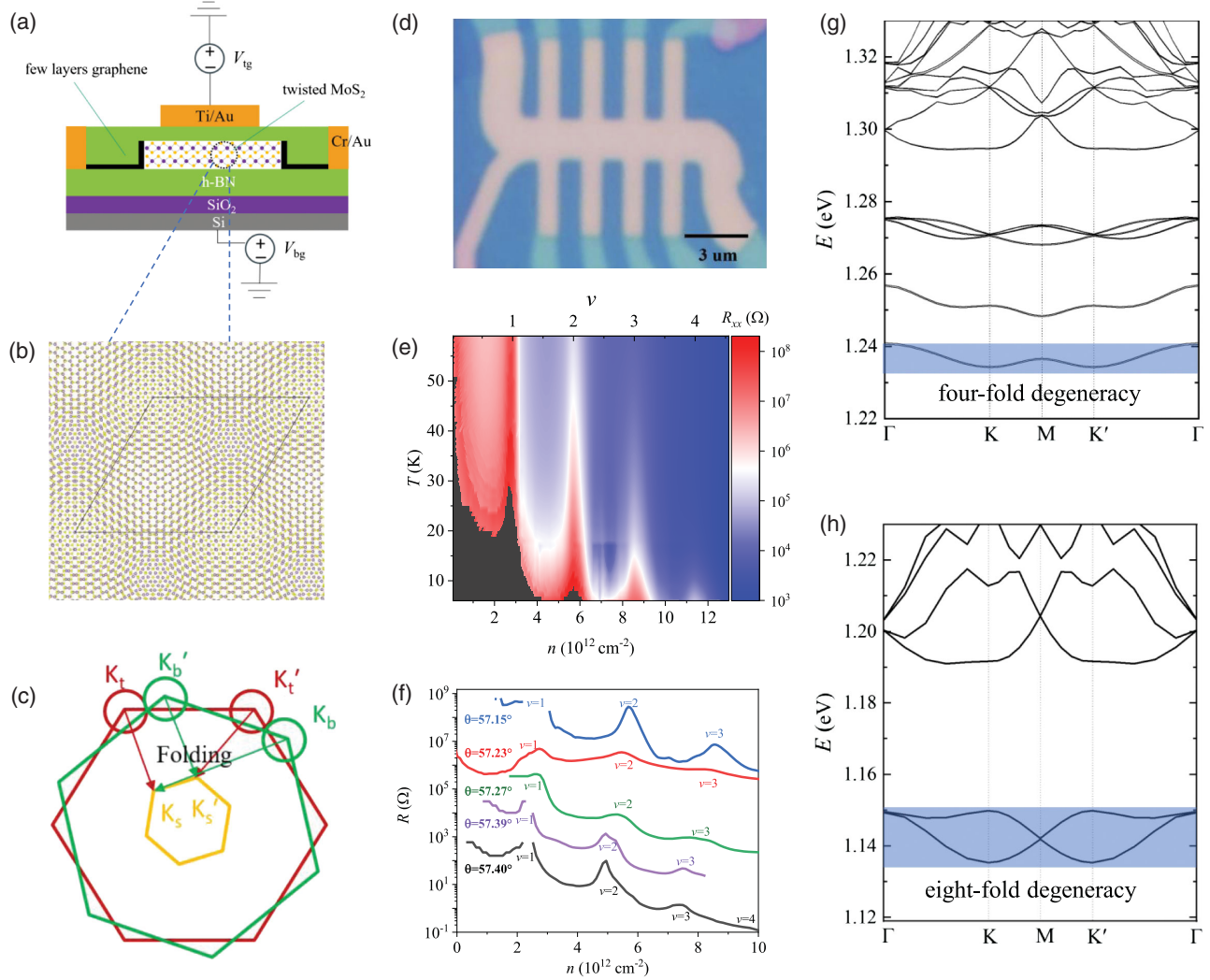


FIG. 1. (a) Schematic of *h*-BN encapsulated twisted bilayer MoS₂ device. (b) Illustration of moiré superlattice formed by $\sim 57.5^\circ$ twisted bilayer MoS₂. (c) Illustration of moiré mini-Brillion zone. (d) Optical image of device No. 1. (e) Color plot of four terminal longitudinal resistance against carrier densities and temperatures of device No. 1, showing four prominent insulating states at $\nu = 1, 2, 3$, and 4. (f) Resistance as a function of n for five twisted bilayer MoS₂ devices. The curves are offset for clarity. (g)–(h) The single-particle energy dispersion of 56.85° twisted bilayer MoS₂ in first mini-Brillouin zone with (g) and without (h) consideration of layer hybridization. The first electron moiré flat miniband is outlined by blue shadow.

This indicates that strong electron-electron interactions exist within flat moiré minibands in twisted bilayer MoS₂, which lift the flavor degeneracy, give rise to full spin-valley polarized flat bands, and drive correlation-induced insulating states at $\nu = 1, 2, 3$.

Interestingly, the presence of correlated insulator states at $\nu = 1, 2, 3$ suggests that the moiré conduction bands of twisted bilayer MoS₂ would emerge as a layer-hybridized SU(4) correlated model simulator. This is in stark contrast to previous TMD moiré superlattice results described by the one-orbital SU(2) Hubbard model (that is, correlation-induced insulating states at integer fillings appear only at half filling of moiré flat band with one hole or electron per superlattice site) [18,22,24] and offer extraordinary opportunities to underpin new phenomena, such as the orbitally

selective Mott phase [41], SU(4) chiral spin liquid, and exciton supersolid phases [42].

Apart from the flat first moiré miniband, DFT calculations also show the second moiré miniband with narrow bandwidth [Fig. 1(g)]. However, no correlated states associated with the second moiré miniband are observed. This is probably due to the additional electrostatic potential and screening effects introduced by the filled charge carriers that result in a small on-site electron-electron Coulomb repulsion and the reduction of correlation effects. It is noteworthy that similar effects have also been observed in MoSe₂/WS₂ moiré superlattices [25].

Possible room-temperature correlated states.—By comparing the band structures with [Fig. 1(g)] and without [Fig. 1(h)] considering the layer hybridization, electronic

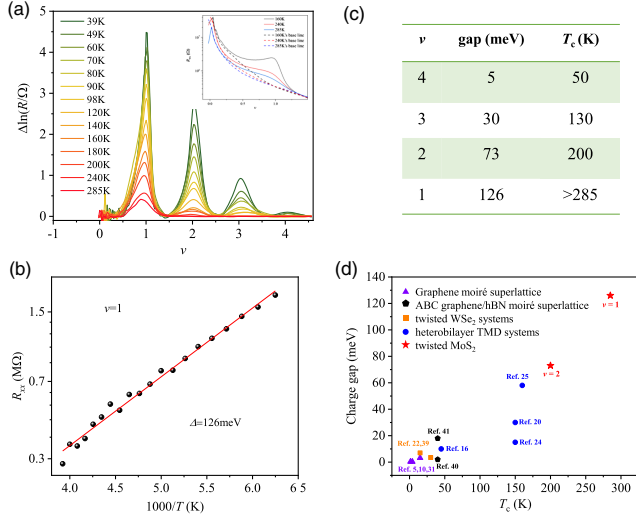


FIG. 2. (a) Four-terminal longitudinal resistance against ν at different temperatures. Inset: the origin data of longitudinal resistances and fitted background resistances as a function of ν at temperatures of 160, 240, and 285 K. (b) Plot of R versus $1000/T$ for $\nu = 1$ correlated insulating state. The extracted thermal excitation gap through the thermal-activation function (red line) is ~ 126 meV. (c) The derived correlated gaps and critical temperature T_c at $\nu = 1, 2, 3$, and 4. (d) Comparison of the correlated gaps and T_c of twisted bilayer MoS_2 with those in various kinds of moiré superlattices previously reported.

bandwidth W is significantly reduced for the former. This indicates the resonantly enhanced interlayer hybridization induced by the perfect band alignment in twisted bilayer MoS_2 , which can strongly amplify the moiré superlattice effects, and may offer the possibility of high-temperature correlated physics [43]. To confirm this, we thus perform temperature dependent transport measurements. Figure 2(a) presents the evolution of insulating states at $\nu = 1, 2, 3, 4$ as a function of temperature. For clarity, the smooth background has been subtracted (Supplemental Material Fig. 12 [27]). Strikingly, for $\nu = 1$ correlated electronic state in twisted bilayer MoS_2 of AB stacking, the resistance peak can persist up to a high temperature of 285 K. Note that even for origin resistance data without subtracting the background, shoulderlike resistance peak can also be observed at 285 K [inset of Fig. 2(a)]. This evidences the possible room-temperature correlated electronic states and a record-high critical temperature T_c over 285 K, much higher than those reported in magic-angle bilayer graphene (e.g., ~ 10 K) [10] and also better than the state-of-the-art results of TMD homo- or heterostructure moiré superlattices (e.g., ~ 150 K) [24]. Similar values of T_c are also confirmed by the R - T curves (Fig. 13 in [27]). The ultrahigh T_c implies that the electron-electron correlations are ultrastrong in the MoS_2 homobilayer moiré superlattice. From the temperature-dependent transport behavior, we can extract the activated gap sizes Δ of the correlated insulating states with a thermal-activation model

$R \propto e^{-\Delta/(2k_B T)}$ (k_B , Boltzmann constant; T , temperature). Figure 2(b) gives the Arrhenius fits to resistance for $\nu = 1$ correlated insulating state. Also see Supplemental Material Fig. 14 [27] for the Arrhenius fits to resistance at $\nu = 2, 3$, and 4. The derived correlated gaps at $\nu = 1, 2, 3$ are 126, 73, and 30 meV, respectively [Fig. 2(c)]. It is noteworthy that both the critical temperature over 285 K and the correlated gap of ~ 126 meV at $\nu = 1$ are the highest values ever achieved among all the moiré superlattice systems [Fig. 2(d)] [5,10,16,20,22,24,25,38,44–48], confirming the giant electron correlations in MoS_2 homobilayer moiré superlattice with strong layer hybridization.

Stacking effects.—In contrast to twisted bilayer graphene, the sublattice symmetry breaking in TMDs endows the distinct moiré superlattices for twist angles near 0° and 60° . Consequently, TMD moiré superlattices of AB and AA stacking orders are expected to exhibit divergent electronic structures and electron-electron Coulomb interactions. To confirm this stacking order-governed moiré effect, we also perform the transport measurements on twisted bilayer MoS_2 with twist angles around 2.5° (four devices are tested). Interestingly, twisted bilayer MoS_2 of AA stacking do not show any correlation phenomena (Figs. 15–16 in [27]), in contrast to the case of AB stacked MoS_2 moiré superlattices. The absence of correlated insulating states in AA stacked MoS_2 moiré superlattices reveals the strong stacking effects on moiré physics and is consistent with the lack of flat conduction bands evidenced by our calculation (Supplemental Material Fig. 8 [27]) and previous multiscale theory [49].

Nonlinear Hall responses.—The ultrastrong electron correlations and possible room-temperature correlated states, in principle, would enable high-temperature quantum phenomena in twisted bilayer MoS_2 , such as second-order nonlinear Hall effect intricately connected with the quantum geometrical property of Bloch wave functions (i.e., Berry curvature dipole) [50,51]. Figure 3(a) shows a schematic diagram for the nonlinear Hall measurements. Figure 3(b) presents the nonlinear Hall voltage $V^{2\omega}$ as a function of moiré filling factors for a 57° twisted bilayer MoS_2 device (device No. 2). Here we show the nonlinear Hall responses at a relatively high temperature of 60 K so that $\nu = 1$ correlated insulating state can be well distinguished. Notably, strong nonlinear Hall responses can be observed near $\nu = 1$ and 2 correlated insulating states. When lowering the temperature (e.g., 30 K), strong nonlinear Hall responses near $\nu = 3$ can also be found (Supplemental Material Fig. 26 [27]). Figure 3(c) shows the $V^{2\omega}$ against the applied current I^ω for filling factor near $\nu = 2$ correlated insulating state at 29 K. $V^{2\omega}$ scales linearly with the square of I^ω and switches sign when terminal of V and I are simultaneously flipped, confirming the nature of second-order non-linear Hall responses. The linear dependence of $V^{2\omega}$ on $(I^\omega)^2$ can also be found near $\nu = 1$ and 3 (Supplemental Material Fig. 27 [27]).

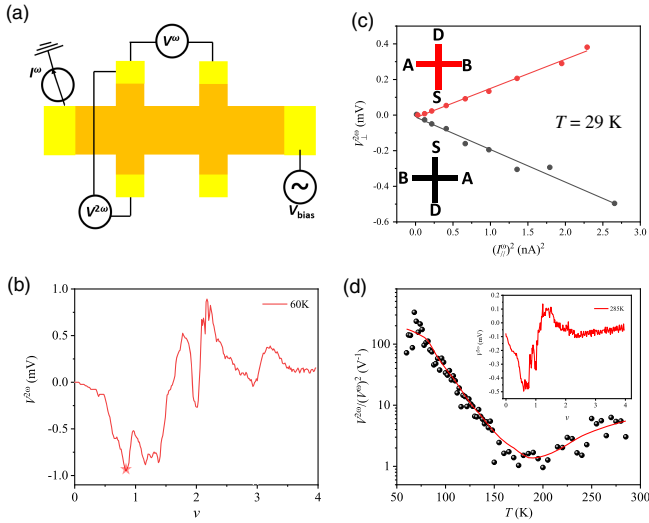


FIG. 3. (a) Schematic diagram of nonlinear Hall measurements. When applying an alternating current I^{ω} with frequency ω , nonlinear Hall voltage $V^{2\omega}$ at frequency 2ω , as well as linear longitudinal voltage V^{ω} , is detected. (b) $V^{2\omega}$ as a function of moiré filling factors for the 57° twisted bilayer MoS_2 device at 60 K. (c) $V_{\perp}^{2\omega}$ versus I_{\parallel}^{ω} for filling factor near $\nu = 2$ at $T = 29$ K. The insets show the electrode geometry for the forward current (red) and backward current (black) directions. The current is injected from the S to D electrodes and the voltage is measured between the A and B electrodes. (d) Temperature dependence of η near filling factor of $\nu = 1$. Inset: $V^{2\omega}$ versus moiré filling factors at 285 K.

Figure 3(d) shows the evolution of nonlinear Hall generation efficiency defined as $\eta = V^{2\omega}/(V^{\omega})^2$ as a function of temperatures near $\nu = 1$. At low temperature, the nonlinear Hall generation efficiency η in twisted bilayer MoS_2 can reach up to 360 V^{-1} , 2 orders of magnitude larger than those in bilayer and few-layer WTe_2 [52,53]. Note that giant nonlinear Hall responses have also been recently observed in twisted bilayer WSe_2 at half filling [54]. With increasing temperature, η gradually decreases. The coincidence of the nonlinear Hall voltage maximum with the correlated insulating states, together with its temperature evolution, reveals that electron correlations play a crucial role in determining Berry curvature dipole and quantum geometry of flat conduction band wave function. Surprisingly, considerable nonlinear Hall responses with $\eta = \sim 1 \text{ V}^{-1}$ can even persist up to room temperature for $\nu = 1$ moiré band filling [inset of Fig. 3(d)]. This further confirms the possible room-temperature correlated insulating state and ultrastrong electron correlations in twisted bilayer MoS_2 of AB stacking. The sizable room-temperature nonlinear Hall responses might be useful to realize technological advances in wireless radiofrequency rectification and frequency doubling.

Conclusions.—We demonstrate the transport evidence of possible room-temperature correlated electronic states and layer-hybridized $\text{SU}(4)$ electron model in twisted MoS_2 homo-bilayer moiré superlattices with twist angles $\sim 57.5^{\circ}$.

Correlated insulating states are clearly observed at moiré band filling factors $\nu = 1, 2, 3$, providing the evidence of a layer-hybridized $\text{SU}(4)$ correlated model. Moreover, electron-electron correlations in twisted bilayer MoS_2 are ultrastrong. The correlated insulating state at $\nu = 1$ hosts a record-large correlated gap of about 126 meV and may persist up to a record-high temperature over 285 K. Additionally, large nonlinear Hall responses up to room temperature are also uncovered in twisted bilayer MoS_2 , demonstrating the quantum geometrical property of electron wave functions. Our results imply that the TMD homobilayer moiré superlattices with resonantly enhanced interlayer hybridization favor as a possible room-temperature correlated quantum system, possessing a promising prospect for a rich phase diagram of high-temperature correlated physics and showing great potential for future technological applications.

We acknowledge support from National Science Foundation of China (NSFC, Grants No. 11834017, No. 12274447, No. 12074412), the National Key Research and Development Program of China (Grants No. 2020YFA0309600, No. 2021YFA1202900, No. 2021YFA1400502), the Strategic Priority Research Program of CAS (Grants No. XDB33000000, No. XDB0470101). K. W. and T. T. acknowledge support from the Elemental Strategy Initiative conducted by the MEXT, Japan (Grant No. JPMXP0112101001), JSPS KAKENHI (Grants No. 19H05790, No. 20H00354, and No. 21H05233) and A3 Foresight by JSPS.

* xianlede@sslabs.org.cn

† wei.yang@iphy.ac.cn

‡ luojun.du@iphy.ac.cn

§ gygzhang@iphy.ac.cn

- [1] E. Y. Andrei, D. K. Efetov, P. Jarillo-Herrero, A. H. MacDonald, K. F. Mak, T. Senthil, E. Tutuc, A. Yazdani, and A. F. Young, The marvels of moiré materials, *Nat. Rev. Mater.* **6**, 201 (2021).
- [2] K. F. Mak and J. Shan, Semiconductor moiré materials, *Nat. Nanotechnol.* **17**, 686 (2022).
- [3] D. M. Kennes, M. Claassen, L. Xian, A. Georges, A. J. Millis, J. Hone, C. R. Dean, D. N. Basov, A. N. Pasupathy, and A. Rubio, Moiré heterostructures as a condensed-matter quantum simulator, *Nat. Phys.* **17**, 155 (2021).
- [4] L. Du, M. R. Molas, Z. Huang, G. Zhang, F. Wang, and Z. Sun, Moiré photonics and optoelectronics, *Science* **379**, eadg0014 (2023).
- [5] Y. Cao, V. Fatemi, A. Demir, S. Fang, S. L. Tomarken, J. Y. Luo, J. D. Sanchez-Yamagishi, K. Watanabe, T. Taniguchi, E. Kaxiras, R. C. Ashoori, and P. Jarillo-Herrero, Correlated insulator behaviour at half-filling in magic-angle graphene superlattices, *Nature (London)* **556**, 80 (2018).
- [6] K. P. Nuckolls, M. Oh, D. Wong, B. Lian, K. Watanabe, T. Taniguchi, B. A. Bernevig, and A. Yazdani, Strongly

- correlated Chern insulators in magic-angle twisted bilayer graphene, *Nature (London)* **588**, 610 (2020).
- [7] Y. Saito, J. Ge, L. Rademaker, K. Watanabe, T. Taniguchi, D. A. Abanin, and A. F. Young, Hofstadter subband ferromagnetism and symmetry-broken Chern insulators in twisted bilayer graphene, *Nat. Phys.* **17**, 478 (2021).
- [8] I. Das, X. Lu, J. Herzog-Arbeitman, Z.-D. Song, K. Watanabe, T. Taniguchi, B. A. Bernevig, and D. K. Efetov, Symmetry-broken Chern insulators and Rashba-like Landau-level crossings in magic-angle bilayer graphene, *Nat. Phys.* **17**, 710 (2021).
- [9] A. T. Pierce, Y. Xie, J. M. Park, E. Khalaf, S. H. Lee, Y. Cao, D. E. Parker, P. R. Forrester, S. Chen, K. Watanabe, T. Taniguchi, A. Vishwanath, P. Jarillo-Herrero, and A. Yacoby, Unconventional sequence of correlated Chern insulators in magic-angle twisted bilayer graphene, *Nat. Phys.* **17**, 1210 (2021).
- [10] X. Lu, P. Stepanov, W. Yang, M. Xie, M. A. Aamir, I. Das, C. Urgell, K. Watanabe, T. Taniguchi, G. Zhang, A. Bachtold, A. H. MacDonald, and D. K. Efetov, Superconductors, orbital magnets and correlated states in magic-angle bilayer graphene, *Nature (London)* **574**, 653 (2019).
- [11] A. L. Sharpe, E. J. Fox, A. W. Barnard, J. Finney, K. Watanabe, T. Taniguchi, M. A. Kastner, and D. Goldhaber-Gordon, Emergent ferromagnetism near three-quarters filling in twisted bilayer graphene, *Science* **365**, 605 (2019).
- [12] Y. Cao, V. Fatemi, S. Fang, K. Watanabe, T. Taniguchi, E. Kaxiras, and P. Jarillo-Herrero, Unconventional superconductivity in magic-angle graphene superlattices, *Nature (London)* **556**, 43 (2018).
- [13] M. Yankowitz, S. W. Chen, H. Polshyn, Y. Zhang, K. Watanabe, T. Taniguchi, D. Graf, A. F. Young, and C. R. Dean, Tuning superconductivity in twisted bilayer graphene, *Science* **363**, 1059 (2019).
- [14] M. H. Naik and M. Jain, Ultraflatbands and shear solitons in moiré patterns of twisted bilayer transition metal dichalcogenides, *Phys. Rev. Lett.* **121**, 266401 (2018).
- [15] H. Li, S. Li, E. C. Regan, D. Wang, W. Zhao, S. Kahn, K. Yumigeta, M. Blei, T. Taniguchi, K. Watanabe, S. Tongay, A. Zettl, M. F. Crommie, and F. Wang, Imaging two-dimensional generalized Wigner crystals, *Nature (London)* **597**, 650 (2021).
- [16] E. C. Regan, D. Wang, C. Jin, M. I. Bakti Utama, B. Gao, X. Wei, S. Zhao, W. Zhao, Z. Zhang, K. Yumigeta, M. Blei, J. D. Carlstrom, K. Watanabe, T. Taniguchi, S. Tongay, M. Crommie, A. Zettl, and F. Wang, Mott and generalized Wigner crystal states in WSe_2/WS_2 moiré superlattices, *Nature (London)* **579**, 359 (2020).
- [17] L. Ma, P. X. Nguyen, Z. Wang, Y. Zeng, K. Watanabe, T. Taniguchi, A. H. MacDonald, K. F. Mak, and J. Shan, Strongly correlated excitonic insulator in atomic double layers, *Nature (London)* **598**, 585 (2021).
- [18] A. Ghiotto, E. M. Shih, G. Pereira, D. A. Rhodes, B. Kim, J. Zang, A. J. Millis, K. Watanabe, T. Taniguchi, J. C. Hone, L. Wang, C. R. Dean, and A. N. Pasupathy, Quantum criticality in twisted transition metal dichalcogenides, *Nature (London)* **597**, 345 (2021).
- [19] T. Li, S. Jiang, B. Shen, Y. Zhang, L. Li, Z. Tao, T. Devakul, K. Watanabe, T. Taniguchi, L. Fu, J. Shan, and K. F. Mak, Quantum anomalous Hall effect from intertwined moiré bands, *Nature (London)* **600**, 641 (2021).
- [20] T. Li, S. Jiang, L. Li, Y. Zhang, K. Kang, J. Zhu, K. Watanabe, T. Taniguchi, D. Chowdhury, L. Fu, J. Shan, and K. F. Mak, Continuous Mott transition in semiconductor moiré superlattices, *Nature (London)* **597**, 350 (2021).
- [21] Y. Xu, K. Kang, K. Watanabe, T. Taniguchi, K. F. Mak, and J. Shan, A tunable bilayer Hubbard model in twisted WSe_2 , *Nat. Nanotechnol.* **17**, 934 (2022).
- [22] L. Wang, E. M. Shih, A. Ghiotto, L. Xian, D. A. Rhodes, C. Tan, M. Claassen, D. M. Kennes, Y. Bai, B. Kim, K. Watanabe, T. Taniguchi, X. Zhu, J. Hone, A. Rubio, A. N. Pasupathy, and C. R. Dean, Correlated electronic phases in twisted bilayer transition metal dichalcogenides, *Nat. Mater.* **19**, 861 (2020).
- [23] F. Wu, L. Li, Q. Xu, L. Liu, Y. Yuan, J. Zhao, Z. Huang, X. Zan, K. Watanabe, T. Taniguchi, D. Shi, L. Xian, W. Yang, L. Du, and G. Zhang, Coupled ferroelectricity and correlated states in a twisted quadrilayer MoS_2 moiré superlattice, *Chin. Phys. Lett.* **40**, 047303 (2023).
- [24] Y. Tang, L. Li, T. Li, Y. Xu, S. Liu, K. Barmak, K. Watanabe, T. Taniguchi, A. H. MacDonald, J. Shan, and K. F. Mak, Simulation of Hubbard model physics in WSe_2/WS_2 moiré superlattices, *Nature (London)* **579**, 353 (2020).
- [25] T. Li, J. Zhu, Y. Tang, K. Watanabe, T. Taniguchi, V. Elser, J. Shan, and K. F. Mak, Charge-order-enhanced capacitance in semiconductor moiré superlattices, *Nat. Nanotechnol.* **16**, 1068 (2021).
- [26] Y. Xu, S. Liu, D. A. Rhodes, K. Watanabe, T. Taniguchi, J. Hone, V. Elser, K. F. Mak, and J. Shan, Correlated insulating states at fractional fillings of moiré superlattices, *Nature (London)* **587**, 214 (2020).
- [27] See Supplemental Material at <http://link.aps.org/supplemental/10.1103/PhysRevLett.131.256201> for details of the electrical performance of van der Waals epitaxial MoS_2 , definition of band edge, twisted angle determination of device No. 1, the displacement field dependence of correlated insulating states, DFT calculation, smooth resistance background subtraction, the R-T curves, Arrhenius fits, stacking effects, possible room temperature correlated states, Hall response and magnetoresistance measurements, rotational symmetry breaking, nonlinear Hall responses at 30 K, nonlinear Hall effects at $\nu = 1, 3$, the displacement field effect of the nonlinear Hall effect, which includes Refs. [18,22,24,28–36].
- [28] Q. Wang, N. Li, J. Tang, J. Zhu, Q. Zhang, Q. Jia, Y. Lu, Z. Wei, H. Yu, Y. Zhao, Y. Guo, L. Gu, G. Sun, W. Yang, R. Yang, D. Shi, and G. Zhang, Wafer-scale highly oriented monolayer MoS_2 with large domain sizes, *Nano Lett.* **20**, 7193 (2020).
- [29] Q. Wang, J. Tang, X. Li, J. Tian, J. Liang, N. Li, D. Ji, L. Xian, Y. Guo, L. Li, Q. Zhang, Y. Chu, Z. Wei, Y. Zhao, L. Du, H. Yu, X. Bai, L. Gu, K. Liu, W. Yang, R. Yang, D. Shi, and G. Zhang, Layer-by-layer epitaxy of multi-layer MoS_2 wafers, *Natl. Sci. Rev.* **9**, nwac077 (2022).
- [30] H. Yu, M. Liao, W. Zhao, G. Liu, X. J. Zhou, Z. Wei, X. Xu, K. Liu, Z. Hu, K. Deng, S. Zhou, J. A. Shi, L. Gu, C. Shen, T. Zhang, L. Du, L. Xie, J. Zhu, W. Chen, R. Yang, D. Shi, and G. Zhang, Wafer-scale growth and transfer of

- highly-oriented monolayer MoS₂ continuous films, *ACS Nano* **11**, 12001 (2017).
- [31] S. L. Li, K. Tsukagoshi, E. Orgiu, and P. Samori, Charge transport and mobility engineering in two-dimensional transition metal chalcogenide semiconductors, *Chem. Soc. Rev.* **45**, 118 (2016).
- [32] G. Kresse, Efficient iterative schemes for *ab initio* total-energy calculations using a plane-wave basis set, *Phys. Rev. B* **54**, 11169 (1996).
- [33] P. E. Blochl, Projector augmented-wave method, *Phys. Rev. B Condens.* **50**, 17953 (1994).
- [34] A. Tkatchenko and M. Scheffler, Accurate molecular van der Waals interactions from ground-state electron density and free-atom reference data, *Phys. Rev. Lett.* **102**, 073005 (2009).
- [35] O. A. von Lilienfeld and A. Tkatchenko, Two- and three-body interatomic dispersion energy contributions to binding in molecules and solids, *J. Chem. Phys.* **132**, 234109 (2010).
- [36] J. Quan, L. Linhart, M.-L. Lin, D. Lee, J. Zhu, C.-Y. Wang, W.-T. Hsu, J. Choi, J. Embley, C. Young, T. Taniguchi, K. Watanabe, C.-K. Shih, K. Lai, A. H. MacDonald, P.-H. Tan, F. Libisch, and X. Li, Phonon renormalization in reconstructed MoS₂ moiré superlattices, *Nat. Mater.* **20**, 1100 (2021).
- [37] K. Kim, M. Yankowitz, B. Fallahazad, S. Kang, H. C. Movva, S. Huang, S. Larentis, C. M. Corbet, T. Taniguchi, K. Watanabe, S. K. Banerjee, B. J. LeRoy, and E. Tutuc, van der Waals heterostructures with high accuracy rotational alignment, *Nano Lett.* **16**, 1989 (2016).
- [38] C. Shen, Y. Chu, Q. Wu, N. Li, S. Wang, Y. Zhao, J. Tang, J. Liu, J. Tian, K. Watanabe, T. Taniguchi, R. Yang, Z. Y. Meng, D. Shi, O. V. Yazyev, and G. Zhang, Correlated states in twisted double bilayer graphene, *Nat. Phys.* **16**, 520 (2020).
- [39] X. Cui, G. H. Lee, Y. D. Kim, G. Arefe, P. Y. Huang, C. H. Lee, D. A. Chenet, X. Zhang, L. Wang, F. Ye, F. Pizzocchero, B. S. Jessen, K. Watanabe, T. Taniguchi, D. A. Muller, T. Low, P. Kim, and J. Hone, Multi-terminal transport measurements of MoS₂ using a van der Waals heterostructure device platform, *Nat. Nanotechnol.* **10**, 534 (2015).
- [40] G.-B. Liu, W.-Y. Shan, Y. Yao, W. Yao, and D. Xiao, Three-band tight-binding model for monolayers of group-VIB transition metal dichalcogenides, *Phys. Rev. B* **88**, 085433 (2013).
- [41] A. Dalal and J. Ruhman, Orbitally selective Mott phase in electron-doped twisted transition metal-dichalcogenides: A possible realization of the Kondo lattice model, *Phys. Rev. Res.* **3**, 043173 (2021).
- [42] Y. H. Zhang, D. N. Sheng, and A. Vishwanath, SU(4) chiral spin liquid, exciton supersolid, and electric detection in moiré bilayers, *Phys. Rev. Lett.* **127**, 247701 (2021).
- [43] D. A. Ruiz-Tijerina and V. I. Fal'ko, Interlayer hybridization and moiré superlattice minibands for electrons and excitons in heterobilayers of transition-metal dichalcogenides, *Phys. Rev. B* **99**, 125424 (2019).
- [44] X. Liu, Z. Hao, E. Khalaf, J. Y. Lee, Y. Ronen, H. Yoo, D. Haei Najafabadi, K. Watanabe, T. Taniguchi, A. Vishwanath, and P. Kim, Tunable spin-polarized correlated states in twisted double bilayer graphene, *Nature (London)* **583**, 221 (2020).
- [45] S. Chen, M. He, Y.-H. Zhang, V. Hsieh, Z. Fei, K. Watanabe, T. Taniguchi, D. H. Cobden, X. Xu, C. R. Dean, and M. Yankowitz, Electrically tunable correlated and topological states in twisted monolayer-bilayer graphene, *Nat. Phys.* **17**, 374 (2021).
- [46] B. A. Foutty, J. Yu, T. Devakul, C. R. Kometter, Y. Zhang, K. Watanabe, T. Takabatake, L. Fu, and B. E. Feldman, Tunable spin and valley excitations of correlated insulators in Γ -valley moiré bands, *Nat. Mater.* **22**, 731 (2023).
- [47] G. Chen, L. Jiang, S. Wu, B. Lyu, H. Li, B. L. Chittari, K. Watanabe, T. Taniguchi, Z. Shi, J. Jung, Y. Zhang, and F. Wang, Evidence of a gate-tunable Mott insulator in a trilayer graphene moiré superlattice, *Nat. Phys.* **15**, 237 (2019).
- [48] J. Yang, G. Chen, T. Han, T. Han, Q. Zhang, Y. Zhang, L. Jiang, B. Lyu, H. Li, K. Watanabe, T. Takabatake, Z. Shi, T. Senthil, Y. Zhang, F. Wang, and L. Ju, Spectroscopy signatures of electron correlations in a trilayer graphene/hBN moiré superlattice, *Science* **357**, 1295 (2022).
- [49] M. H. Naik, S. Kundu, I. Maity, and M. Jain, Origin and evolution of ultraflat bands in twisted bilayer transition metal dichalcogenides: Realization of triangular quantum dots, *Phys. Rev. B* **102**, 075413 (2020).
- [50] S. Sinha, P. C. Adak, A. Chakraborty, K. Das, K. Debnath, L. D. V. Sangani, K. Watanabe, T. Taniguchi, U. V. Waghmare, A. Agarwal, and M. M. Deshmukh, Berry curvature dipole senses topological transition in a moiré superlattice, *Nat. Phys.* **18**, 765 (2022).
- [51] I. Sodemann and L. Fu, Quantum nonlinear Hall effect induced by Berry curvature dipole in time-reversal invariant materials, *Phys. Rev. Lett.* **115**, 216806 (2015).
- [52] Q. Ma *et al.*, Observation of the nonlinear Hall effect under time-reversal-symmetric conditions, *Nature (London)* **565**, 337 (2019).
- [53] K. Kang, T. Li, E. Sohn, J. Shan, and K. F. Mak, Nonlinear anomalous Hall effect in few-layer WTe₂, *Nat. Mater.* **18**, 324 (2019).
- [54] M. Huang, Z. Wu, J. Hu, X. Cai, E. Li, L. An, X. Feng, Z. Ye, N. Lin, K. T. Law, and N. Wang, Giant nonlinear Hall effect in twisted bilayer WSe₂, *Natl. Sci. Rev.* **10**, nwc232 (2023).